Journal of Mining and Environment (JME) Vol. 12, No. 4, 2021, 1089-1102

Shahrood University of Technology

Iranian Society of Mining Engineering (IRSME)

Journal of Mining and Environment (JME)

journal homepage: www.jme.shahroodut.ac.ir

THOMSON REUTERS

An Experimental and CFD Investigation on Effect of Initial Bubble Diameter on its Rise Velocity Profile in A Laboratory-Scale Flotation Column Cell

Narjes Khorasanizadeh[1], Mohammad Karamoozian[1*] and Hossein Nouri-Bidgoli[2]

1- Faculty of Mining, Petroleum & Geophysics Engineering, Shahrood University of Technology, Shahrood, Iran
2- Department of Mechanical Engineering, Islamic Azad University of Kashan, Kashan, Iran

Article Info

Received 15 September 2021
Received in Revised form 25 November 2021
Accepted 6 December 2021
Published online 6 December 2021

DOI:10.22044/jme.2021.11213.2101

Keywords

Column flotation
Bubble diameter
Velocity profile
Multi-Phase simulation
CFD simulation

Abstract

The bubble diameter effect on the bubble rise velocity profile in a flotation column is studied by the two-phase computational fluid dynamics (CFD) method. The simulations are done in the ANSYS® Fluent® software using a two-phase volume of fluid model. The computational domain is a square cross-section column with a 10 cm width and a 100 cm height, in which air is interred as a single bubble from the lower part of the column by an internal sparger. An experimental test is also performed, the hydrodynamics parameters are recorded, and the simulated results are validated using the values obtained for the bubble rise velocity. The simulation results obtained indicate that CFD can predict the bubble rise velocity profile and its value in the flotation column with less than 5% difference in comparison with the experimental results. Then the simulations are repeated for the other initial bubble diameter in the bubbly flow regime in order to study the bubble diameter effect on the rise velocity profile. The results obtained demonstrate that the larger bubbles reach the maximum velocity faster than the small ones, while the value of maximum velocity decreases by an increase in the bubble diameter. These results can be used to improve the flotation efficiency.

1. Introduction

With the decline of minerals in the present age, the maximum usage of natural resources and mines has become very important, and this has made mining and the related industries to have a special place in the economy. Therefore, increasing the efficiency of processing operations and optimizing the related systems is of particular importance. Understanding the mechanism and manner of performing physical processes is effective in improving the performance of a system. Fluid science and, in particular, Computational Fluid Dynamics (CFD) is a tool in this regard. The hydrodynamic components have a significant effect on the column flotation process efficiency, and CFD, as a numerical method, can help analyze and predict the flow components. So far, examples of CFD simulations have been performed on the mineral processing equipment with different approaches and objectives [1]. The following is a summary of the studies performed on the flotation column collection area using the CFD simulation method.

The first published work concerning the application of computational fluid dynamics to simulate flotation columns was reported by Deng et al, and a two-dimensional fluid dynamic model was developed to simulate liquid and gas flow patterns in a flotation column. Laminar flow was considered in the study and drag force was considered between water and air bubbles. The presence of a circulating flow structure in the flotation column was revealed to be one of the primary reasons for mixing in column flotation [2]. To avoid circulating flow structure and obtain good

Corresponding author: m.karamoozian@shahroodut.ac.ir (M. Karamoozian).

mixing, Xia et al studied the liquid-gas flow in the open, baffled and packed flotation columns. The fluid motion was simulated by directly solving the two-dimensional Navier-Stokes equations using a SIMPLE approach and motions of bubbles were modelled by the Lagrangian equation. The results showed the inclusion of horizontal baffles or corrugated packings could dampen the back-mixing but cannot totally remove detrimental vortexes in the column [3].

Chakraborty et al used a standard k-ε model were used to model the turbulence in the continuous phase. An Eulerian-Eulerian model was used to simulate the gas-liquid two-phase flow in the flotation column. It was found that increasing air flow rate resulted in an increase in gas holdup and complexity in the plume structure [4]. Nadeem et al studied the collision probabilities of fine particles with bubbles at intermediate Reynolds number using a stationary bubble and down co flowing particles [5].

Flotation kinetics in the flotation columns were not computationally simulated until Koh and Schwarz studied the cell hydrodynamics in a Microcell column and Jameson cell in relation to bubble-particle attachment and detachment. It was found that the local value of bubble-particle detachment rate was directly related to the local turbulent dissipation rate [6].

Also, Rehman et al have done an investigation on the effect of various baffle designs on air holdup and mixing in a flotation column using axisymmetrical geometry [7]. An increase in turbulence in the tank was shown to decrease the maximum floatable size of particles by Sahbaz et al where the high turbulent region and its effect on the upper floatable size limit in the Jameson cell were studied. The results showed two main turbulent regions of the mixing zone in the upper part of the downcomer and the critical region at the separation tank [8]. Yan et al used a standard k-ε model to simulate single-phase flow in a cyclonic-static micro-bubble flotation column. Flow patterns in different parts such as separation unit and cyclonic unit were analyzed to strengthen the design of each unit. It was shown that the radial and tangential velocity in the column flotationdecreased and the axial velocity became more homogeneously distributed [9].

Instead of using a standard k-ε model, Gong et al compared three different turbulence models, a standard k-ε, a RNG k-ε and a realizable k-ε turbulence model, in the study of the distributions of velocity, pathlines, turbulent intensity and turbulent kinetic energy. The results showed a consistent decreasing in the intensities of velocity and turbulence from the wall to the center of the column and from the bottom of the column to its top [10]. Comparatively, Wang et al compared three turbulence models, standard k-ε model, RSM-S model and RSM-L model, and results were compared to PIV measurements of velocity distributions along the radius and RSM-S turbulence model gave the closest prediction. Cone angle at 48 degrees was found optimal to generate the desired relatively static environment in the column flotation section [11].

The coalescence and break-up of bubbles were modeled with a population balance model by Sarhan et al, where an Eulerian-Eulerian approach was used to investigate the influence of the concentration of solid particles on bubble coalescence in a flotation cell. It was found that gas holdup increased with increasing gas velocity [12]. Cai et al used a population balance model in the study of oil-water separation characteristics in a flotation column. Liquid and oil droplet flows were studied using an Eulerian-Eulerian approach. It was found that the efficiencies of coalescence and breakage of oil droplets were effectively promoted by increasing turbulence intensity since the kinetic energy of oil droplets was given by liquid turbulent kinetic energies [13, 14].

Sarhan et al studied the effect of bubble-particle aggregate density on the flow dynamics [15]. They further studied the effect of particle type, density, wettability and concentration on gas holdup and bubble hydrodynamics. It was found that the addition of hydrophobic particles to the air/water mixture promotes bubble coalescence and, therefore, reduces the gas holdup, while the addition of hydrophilic particles suppresses bubble coalescence and increases the gas holdup [16].

Zhang et al studied the effect of packed fluid guiding media in the column using a single-phase model. The improvement in the flotation recovery in a packed flotation column was connected to the changed hydrodynamics where particles attached to bubbles efficiently in the strong cyclonic flow and the newly formed bubble-particle aggregates can quickly report to the froth zone [17].

Wang et al applied CFD simulations to study the effect of vortex generators on the turbulence kinetic energy and the turbulence dissipation rate in a pipe flow unit of a cyclonic-static micro-bubble

flotation column. A lab-scale experiment was carried out to validate the flotation performance of proposed arrangements. It was shown that the modified structures could improve flotation performance by enhancing the yield and the combustible recovery [18, 19].

The effects of a vertical baffle on the axial mixing in a flotation column was studied by Farzanegan et al and it was shown that the baffle divided the flotation column into two parallel columns [20]. Yang et al investigated the effect of elevated pressure on the bubble breakage and gas holdup with a CFD-PBM coupled model [21]. To study the effects of superficial gas velocities and particle type, density, wettability and concentration on S_b and bubble concentration in three-phase flow dynamics in flotation column Sarhan et al used Eulerian mole coupling with k- ε model [22].

The flow field, gas dispersion, and solids concentration in a flotation cell fitted with an Outotec (Outokumpu) Flotation mechanisms have been studied using both experimental and multi-phase (CFD) modeling. The velocity field of the liquid phase was measured using (LDV) in Schwarz et al research [23]. Nasirimoghaddam et al provided a kinetic model for estimating column flotation rate constant using Eulerian-Eulerian multiphase and Realizable k- ε turbulent model [24].

Yang et al performed a modeling study to further unravel the governing mechanisms occurring developing a CFD-PBM model in a DAF tank [25]. Yan et al measured the cross-section and axial section of gas-liquid two-phase flow field in a lab-scale cyclonic flotation column, particle image velocimetry (PIV) is combined with endoscopic measurement and phase discrimination technique [26].

In these research works, most attempts have been made to investigate the overall flotation operations. However, due to the special role of bubbles in floating the selected particles and transporting them to the froth phase, and to better understand the effect of the hydrodynamic components, more studies should be conducted on them.

According to the preceding studies, air bubbles' dynamic behavior in two-phase flow in flotation has been investigated in many research works, while some main features of bubble dynamics in the flotation process such as the effect of the initial bubble diameter on the bubble rise velocity are still not well-understood. The purpose of this work is to investigate the rise velocity profile of different bubble diameters in a single-bubble system by the use of video processing techniques in order to create an insight into the dynamics of the bubble in the flotation process.

2. Methodology

In order to achieve a reliable result in simulation, at first, a complete understanding of the governing physics phenomenon is a need, and secondly, selection of suitable physical models (multi-phase model, turbulence model, etc) is required to apply in the simulation tools (e.g. Fluent software). Therefore, this study has been defined and carried out concerning the undeniable importance of improving the efficiency of flotation as the most efficient separation unit and developing the sciences related to flotation in both the experiment and simulation. In the first step, in order to simplify the problem, the motion of a single bubble is investigated experimentally and numerically, and then the bubble rise velocity profile and the effect of initial bubble diameter are studied.

Afterward, first, the experimental test is explained in detail, and then the method used in the simulation and its steps are fully described. The experimental and simulation results are presented, and by comparing them, the numerical values are validated. Finally, the rise velocity profile of the bubble and the bubble diameter effect on it are discussed.

2.1. Experiment

A laboratory flotation column was constructed, and an experimental test was done in order to get the required experimental values for simulation of the prediction's validation. In the next sub-sections, the flotation column characteristics and setup are explained.

2.1.1. Column flotation cell characteristics and setup

Column dimensions: the 1 (m) high flotation column by a square cross-section with 10 (cm) crosswise and a height to diameter ratio of 7.14 was used, shown schematically in Figure 1. The square cross-section makes it easy to record the experimental observations. The column material was selected from clear Plexiglas with a thickness of 5 mm because it was strong and light; also its transparency allowed to observe the process.

This system was equipped with an internal sparger including a pneumatic hose with a diameter of 2 mm, which was located in the lower part of the column at a height of 4 cm, and the automatic air

pump (ACD-500) with a power of 5 W, a pressure of 0.012 MPa, and the capacity to inject 3 L of air per minute was employed for aeration. The bubble enters the system individually. In fact, the time interval between the entries of two consecutive bubbles into the column was adjusted in the way that the bubble's velocities were not affected by their frequency. Since the inlet airflow to the column was very small in these conditions, it was not possible to use the conventional airflow measuring instruments. Therefore, in order to adjust the inlet airflow to the column, a needle valve was used after the pump.

The experiment was performed at the atmospheric pressure and air temperature of 30 ± 0.5 (°C). The experiments were done in order to investigate the hydrodynamic conditions in the flotation column in the presence of two phases, gas and liquid. Therefore, firstly, the column was full of water to a height of 90 (cm) (considering the possible flow fluctuations), and then the air valve was opened and air entered the column.

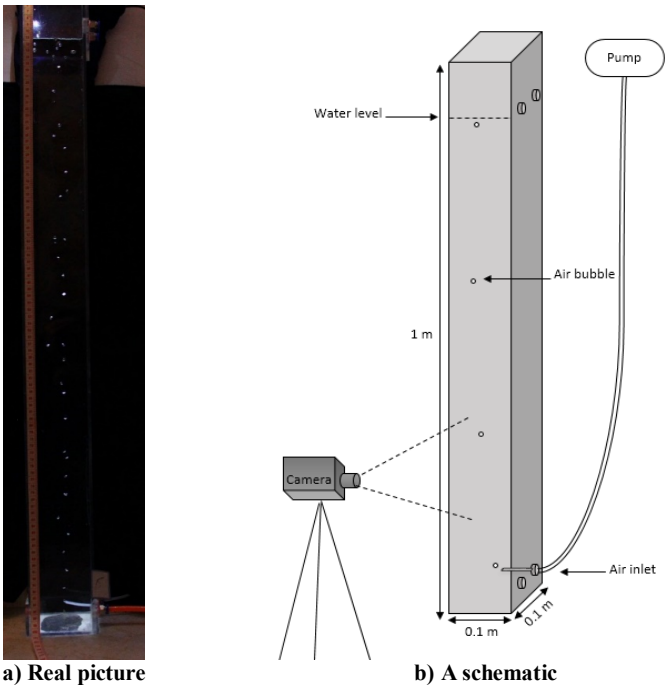

a) Real picture **b) A schematic**

Figure 1. Experimental setup.

2.1.2. Image analysis

After ensuring the stability of the flow in the column, imaging of the column and recording the results was performed using a Canon EOS 500d. The video recording speed was 30 frames per second, and the continuous shooting speed was 3.4 frames per second. Figure 2 summarizes the imaging process and the purpose of doing it, which is explained in the following:

- Measuring bubble diameter: For this purpose, the image of the bubble was recorded in the inlet, then Digimizer[1] defined a unit of measurement from the ruler installed on the column wall, and the diameter of the bubble was measured from the image. In order to calculate the bubble diameter, a volumetric equivalent diameter was calculated according to Equation (1) [27].

$$d_{eq} = (hb^2)^{1/3} \quad (1)$$

where:

d_{eq}	is the volumetric equivalent diameter (m)
h	is the smallest diameters of the bubble (m)
b	is the largest diameters of the bubble (m)

- Measure the bubble displacement in two consecutive photos, and calculate the bubble rise velocity: in order to measure the bubble rise velocity value, the camera's continuous shooting mode settings are used. By measuring the

[1] Digimizer is a flexible software package that is very useful for analyzing the images, and allows you to manually accurately measure the components of images.

displacement of a bubble in two consecutive images and considering the time interval between two images (1/3.4 = 0.29 s), the velocity of the bubble was calculated. For this purpose, the photos were taken in four sections from 0 to 20 (cm), 20 to 45 (cm), 45 to 70 (cm), and (70) to 90 (cm). Figure 3 shows the bubble displacement in two consecutive photos of bubble rise in the column.

- Counting the number of bubbles in the column and calculating the gas holdup: An overall view of the column was taken, and the number of bubbles inside the column was counted. By multiplying the number of bubbles that present simultaneously in the column in the volume of one bubble, the total volume of air in the column was obtained, and by dividing it by the volume of water of the column, the gas holdup was calculated.
- Counting the number of interred bubbles to the column per second; in order to measure the inlet air flow rate to the column, in stable conditions, the location of the sparger was filmed, the number of interred bubbles to the column was counted per unit time, and by considering the volume of bubbles, the inlet air flow rate was calculated.

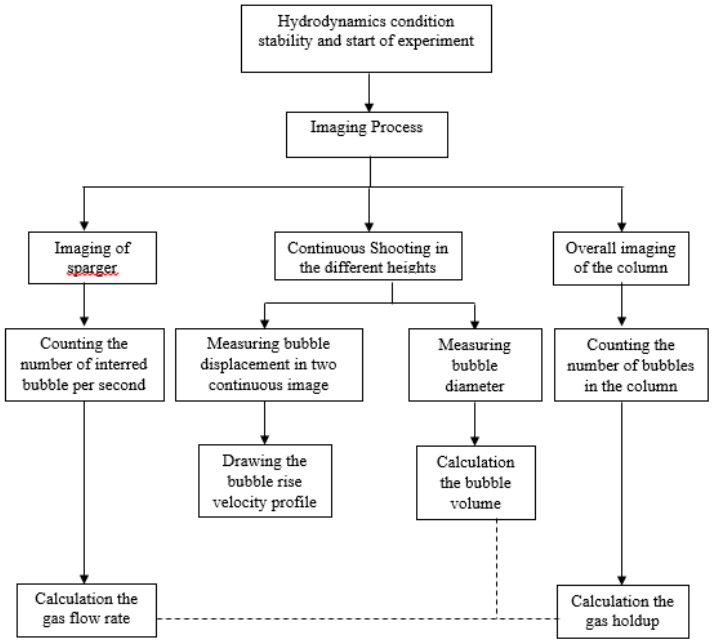

Figure 2. Image analysis diagram used in experimental tests.

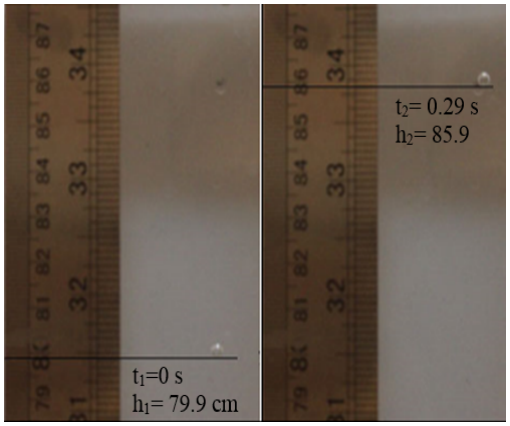

Figure 3. Bubble displacement in two consecutive photos of bubble rise in the column.

2.2. Modeling and simulation

The geometry and meshing were generated by Gambit® 2.4.6, and then the flow calculations were done by ANSYS® Fluent® 15.0 on a computer system with a Xeon processor consisting of 42 cores used in parallel mode. The details of the modeling procedures are presented in the following sub-sections.

2.2.1. Governing equations

The Volume Of Fluid (VOF) model was used in this work as a multi-phase model in order to simulate a bubble motion in the water, which is an advection scheme and a numerical recipe that allows the programmer to track the shape and position of the interface. The movement of the gas-liquid interface was tracked based on the distribution of the gas volume fraction in a computational cell, while the interfacial mass transfer was neglected. Equations (2) and (3)

represent the mass and momentum equation for the two-phase flow:

$$\nabla.(\rho\vec{v}) = 0 \quad (2)$$

$$\frac{\partial}{\partial t}(\rho\vec{v}) + \nabla.(\rho\vec{v}\vec{v}) = -\nabla p + \nabla.\ \tau\ + \rho\vec{g} + \vec{F} \quad (3)$$

where:

ρ	is the density (kg/m^3)
$\vec{v}$	is the velocity vector (m/s)
p	is the scalar pressure value (Pa)
τ	is the tensor of viscous stress (Pa)
$\vec{g}$	is the gravitational acceleration (m/s^2)
$\vec{F}$	is the surface tension source term (N/m^2)
t	is the time (s)

In a two-phase system, the phases are signified by the subscripts *g* and *l;* the density and viscosity in each cell are given by Equations (4) and (5) [28]:

$$\rho = \alpha_g\rho_g + \alpha_l\rho_l \quad (1)$$

$$\mu = \alpha_g\mu_g + \alpha_l\mu_l \quad (2)$$

where:

ρ	is the density (kg/m^3)
α_g	is the volume fraction of gas-phase (%)
ρ_g	is the gas density (kg/m^3)
α_l	is the volume fraction of liquid-phase (%)
ρ_l	is the liquid density (kg/m^3)
μ	is the viscosity (Pa.s)
μ_g	is the viscosity of gas (Pa.s)
μ_l	is the viscosity of liquid (Pa.s)

The interface tracking between two phases was done by the solution of a continuity equation for the volume fraction of gas, which is described in Equation (6):

$$\frac{\partial\alpha_g}{\partial t} + \vec{v}.\nabla\alpha_g = 0 \quad (6)$$

where:

α_g	is the volume fraction of gas-phase (%)
$\vec{v}$	is the velocity vector (m/s)
t	is the time (s)

The liquid volume fraction was calculated based on Equation (7) [24]:

$$\alpha_g+\alpha_l=1 \quad (7)$$

where:

α_g	is the volume fraction of gas-phase (%)
α_l	is the volume fraction of liquid-phase (%)

2.2.2. Geometry

The geometry was made according to the laboratory flotation column described in the experimental section. Based on what was seen in the experiments, the movement of a single bubble and its rise path almost was located in the column's middle, and the distance of the bubble from the walls was long enough that the bubble's movement was not affected by the wall. Therefore, the flow was assumed to be linear, and the simulations were performed in two dimensions. The schematic representation of the geometry and the boundary conditions are shown in Figure 4.

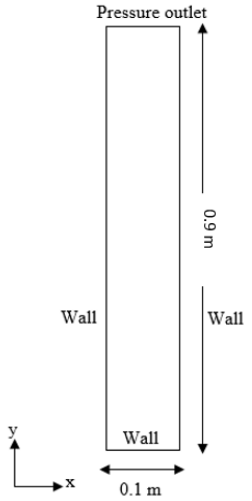

Figure 4. Schematic of column geometry used in experiments and simulations.

2.2.3. Meshing

After generating the geometry in the Gambit software, a meshing operation was performed. The desired mesh was quad, and the criterion of meshing was located 20 to 30 cells in the bubble diameter direction. Since the range of transverse oscillation of the bubble was (2* (d_{bubble} + $0.5d_{bubble}$)), so for, meshing the column's width was divided into three parts: the column's middle, in which the bubble was interred and begun to oscillate in an upward motion; and two parts on the

sides. In the bubble rise path-the middle part of the column-the grid was smaller [29].

2.2.4. Simulation and boundary conditions

In this section, choosing and setting simulation and boundary conditions such as the transient flow time step, two-phase model, convergence criteria, and discretization scheme are mentioned.

- Transient flow: The purpose was to study the components related to the bubble motion so all simulations were done time-dependent.
- Time step: In solving the problem transiently, it was necessary to divide the processing time into small parts. A good way to determine the amount of time step was to observe the number of iterations done in each time step to achieve convergence. The appropriate number of repetitions in each time step was 10 to 30 [30]. In this research work, the variable time step was used. Thus the calculations start with the time step of 10^{-8} (s), and based on the value determined for the courant number (0.5) could be increased to 10^{-4} (s). It is necessary to mention two points: firstly, the mentioned values were used only based on the author's experience, and secondly, it had the maximum accuracy that could be used according to the available hardware for the authors.
- Laminar flow: Since the motion of a single bubble was studied, the flow was laminar, and the turbulence model was not applied [31].
- Two-phase flow: All simulations were performed by considering two phases: water and air as the primary and the second phase. The fluid's properties used in the simulation at a temperature of 30 ± 0.5 ˚C (the experimental temperature) are shown in Table 1. Also the value of surface tension was considered to be 0.0712 (N/m). It should be noted that since the ratio of minimum diameter to the maximum diameter was less than 1%, the interred bubble was considered to be spherical [23].
- Gravity Acceleration: In all simulations, a value of 9.81 (m/s^2) was intended for gravitational acceleration in the y-direction.
- Convergence criteria: The normalized residual values, for continuity less than 10^{-3} and volume fraction less than 10^{-6}, were considered as the convergence criteria.
- Discretization scheme: The first-order upwind scheme was used for the momentum equations, whereas the discretization of the volume fraction equation was performed using the QUICK scheme. The algorithm was used to couple the velocity fields, and the pressure was PISO.

Table 1. Properties of fluid used in the experiments and simulation [32].

	μ (kg/m.s)	ρ (kg/m^3)
Water	0.799e-3	996
Air	1.872e-5	1.164

2.2.5. Mesh verification

The mesh independence of the solution was done by studying the bubble rise velocity. In this way, the mesh numbers along the bubble diameter and consequently the other parts of the computational domain increased to the extent that the values obtained from the simulation had the least difference with the experimental results. Table 2 shows three different mesh numbers used for this purpose. Figure 5 shows the bubble rise velocity profile of these simulations results.

Table 2. Different mesh numbers to examine the mesh verify in the simulations.

	Mesh number in the bubble diameter direction	Mesh number in the middle	Mesh number in every side	Mesh number in the height	Total mesh number
Mesh 1	20	63	100	6250	493,750
Mesh 2	24	75	200	7500	762,500
Mesh 3	28	88	300	8750	1,070,625

As shown in Figure 5, the meshes 2 and 3 predict the velocity pattern more similar to the experimental results than the mesh number 1. The numerical values also show that by decreasing the mesh number and using mesh 3 in the simulations, the velocity values change slightly. Therefore, with an approximation of less than 2%, mesh 2 was selected and used in the simulations.

decrease in the bubble diameter. In the following result of the experiment, the validation details and discussion about the result obtained are provided.

3. Results and discussion

An experimental test and the CFD simulations were performed in the mentioned conditions. After validation of the numerical values, the simulations were performed again with a 20% increase and

3.1. Experimental results

Since the optimal performance of the column was in a bubbly flow regime [33], the gas holdup variation concerning the superficial velocity of gas had to be considered for all bubble sizes that could be produced by the experimental equipment. The values of superficial gas velocity were calculated for all the experiments by dividing the airflow rate to column cross-section area, and presented in Figure 6. As shown in this figure, whenever the superficial velocity of gas reaches 2.9e-4 cm/s (matching to 3.5 mm of the bubble's diameter), gas holdup comes to be unsteady and the turbulent flow starts.

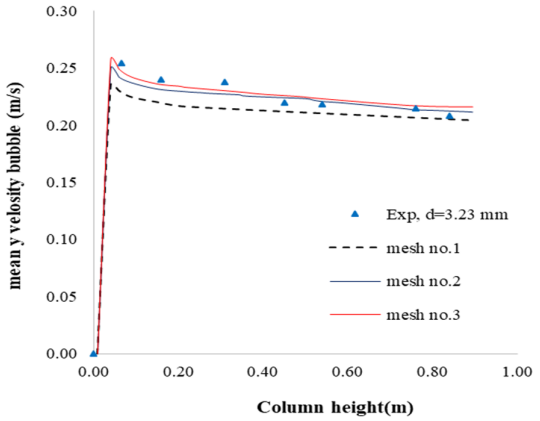

Figure 5. Comparison of Bubble rise mean velocity profile in the experimental test and simulations by different mesh numbers.

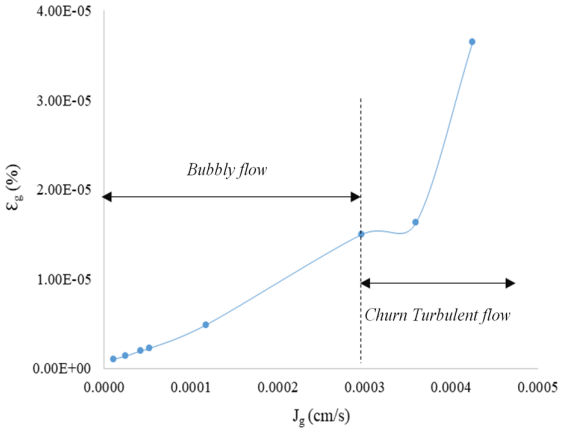

Figure 6. Bubbly flow diagram in the experimental tests.

Therefore, the velocity measurements were done for the bubbles with a diameter of 3.23 mm, and the results obtained were used to validate the initial simulation result. Table 3 shows the hydrodynamic variables of the column, which were measured and calculated according to the algorithm presented in Figure 2.

The other bubble sizes in the bubbly flow regime (2.60, 2.87, 3.23, and 3.50 mm) were used for the additional simulations to study the how bubble size affects the velocity profiles.

Table 3. The experimental results.

Bubble diameter (m)	Bubble volume (m^3)	Number of an incoming bubble per second	Airflow rate (m^3/s)	Number of the bubble in the column	The total volume of air in the column (m^3)	Gas holdup (%)	superficial gas velocity (m/s)
0.00323	1.76E-08	0.24	4.2E-09	1.0	1.76E-08	1.96E-06	4.23E-07

3.2. Dimensionless numbers

Dimensionless numbers represent the behavior of the fluid flow, and are very important in fluid mechanics. In this work, the Reynolds, Morton, and Eotvos numbers were used to determine the bubble shape using the Clift diagram. A brief description of these numbers and their equations are in the following:

- Reynolds number: A quantity without a significant unit was used in fluid mechanics in order to predict the flow pattern. This number is the ratio of the inertial force to the viscous force. The Reynolds numbers tend the flow to have a laminar, layered pattern, while in high Reynolds numbers, the flow becomes turbulent and its value is obtained by Equation 8.

$$\mathrm{Re} = \frac{\rho_l . u_b . d_b}{\mu_l} \quad (8)$$

where:

Re	is the Reynolds number
ρ_l	is the liquid density (kg/m^3)
u_b	is the velocity of the bubble (m/s)
d_b	is the diameter of the bubble (m)
μ_l	is the liquid viscosity (kg/m.s)

- Morton number: A number to describe the bubble shape moving in a fluid, and is described as the Equation 9.

$$\mathrm{Mo} = \frac{g.\mu_l{}^4}{\rho_l.\sigma^3} \quad (9)$$

where:

Mo	is the Morton number
g	is the gravity acceleration (m/s^2)
μ_l	is the viscosity of the liquid (kg/m.s)
ρ_l	is the density of the liquid (kg/m^3)
σ	is the surface tension (Pa)

- Eotvos number: The ratio between the internal force and the surface stress acting on the surface between the two phases. According to the definition, its value is obtained by the Equation 10. [34]:

$$Eo = \frac{g(\rho_l - \rho_g)d^2}{\sigma} \quad (10)$$

where:

Eo	is the Eotvos number
g	is thehe gravity acceleration (m/s^2)
ρ_l	is the density of the liquid (kg/m^3)
ρ_g	is the density of the gas (kg/m^3)
d_b	is the bubble diameter (m)
σ	is the surface tension (Pa)

The values of the dimensionless numbers for the bubble diameter of this work are provided in Table 4.

3.3. Validation

The next step was the validation of the simulation results by comparing the numerical and experimental values. In the experiment, the bubble velocity was calculated by measuring its displacement in two continuous shots, and due to the time interval between two continuous shots, a mean velocity was achieved. Also in the simulation, a mass center was defined for the bubble, and the value of the mean velocity was calculated according to its displacement in the defined height per unit time. Figure 7 shows the bubble mean velocity profile for a bubble with a 3.23 mm initial diameter based on numerical simulations and experimental measurements. As it could be seen, the bubble mean velocity profile had two parts; in the first part, the bubble velocity was increasing immediately, and in the second part, it decreased with a descending acceleration. At the start of the movement, the axial component of the bubble velocity was zero but by the effect of the buoyancy force, which was the main cause of the bubble movement, it reached its maximum value after a very short time; then a continuous decrease in bubble rise velocity was seen [35].

Also the velocity values recorded in the experimental test and the predicted values in the simulation, and the difference between the two are given in Table 5. As it could be seen, the simulation predicts the bubble mean velocity with less than a 5% difference in comparison with the experimental values.

Table 4. The values of dimensionless numbers according to the experimental test.

Bubble diameter (m)	Re	Eo	Mo
0.0026	617.19	0.93	
0.0032	766.74	1.43	1.112E-11
0.0038	887.80	1.92	

Table 5. Comparison of experimental and numerical bubble mean velocities.

Bubble diameter (mm)	Height (m)	Mean velocity (m/s) Exp.	Mean velocity (m/s) Sim.	Difference (%)
3.23	0.066	0.254	0.250	1.60
	0.16	0.240	0.231	3.90
	0.31	0.238	0.227	4.85
	0.45	0.220	0.221	0.45
	0.54	0.218	0.220	0.91
	0.76	0.215	0.214	0.47
	0.84	0.208	0.210	0.95

Figure 8 shows the approximate range of the Eotvos and Reynolds numbers for different bubble sizes. Examination of the values of these dimensionless numbers for the bubbles with equal diameters 2.6 to 3.8 mm confirms the accuracy of the values measured and recorded in the present work.

Furthermore, the location of the bubble in the Clift diagram (pattern of deformation bubble rising in the liquid column) was investigated as a qualitative validation, and was compared with the real picture of bubble shape in the experimental test and the shape of the bubble in the CFD simulation snapshot, for a bubble with 3.2 mm diameter rising in the height of 50 cm of the column (Figure 9). In the bubble size range of the present work, with increasing bubble diameter, Reynolds increases, and the surface tension force decreases; other forces (viscosity, inertia, and compressive dynamics) increase, and the bubble shape changes from spherical to elliptical, and then more increasing in the bubble diameter making a spherical cap in the bubble shape [23].

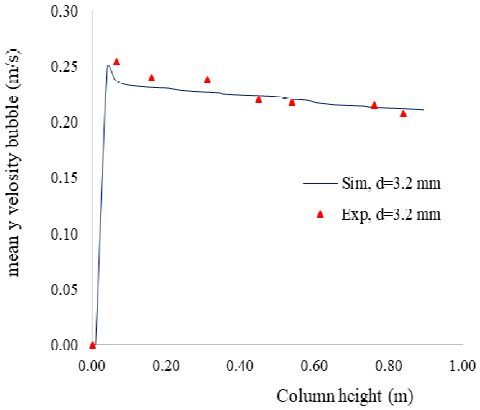

Figure 7. Comparison of experimental and numerical bubble mean velocity (d = 3.23 mm).

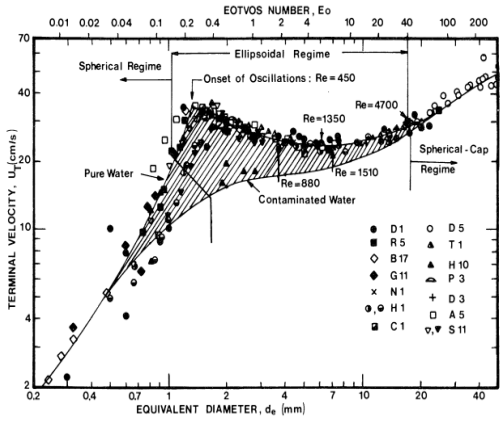

Figure 8. Terminal velocity of air bubbles in water at 30° C [27].

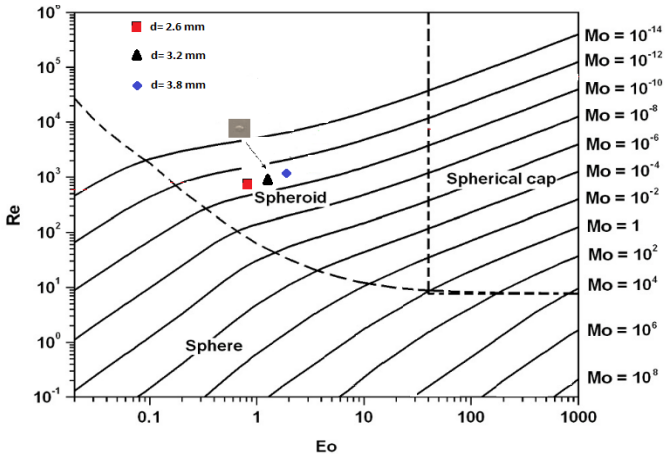

a) Clift diagram

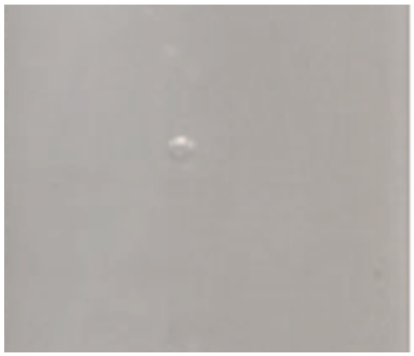

b) Real picture of bubble shape in experimental test

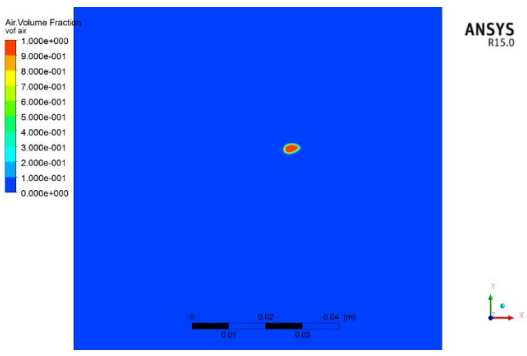

c) A CFD snapshot of bubble shape

Figure 9. The bubble shape rising in the column a) according to the dimensionless number in the Clift diagram [27], b) Real picture of the bubble in the experimental test, and c) Simulation snapshot for a bubble with 3.2 mm diameter rising in the height of 50 cm of the column.

3.4. Effect of initial bubble diameter on bubble rise velocity profile

In order to investigate that how the bubble rise velocity profile is affected by the initial bubble diameter, the simulations were repeated for the other bubble diameters mentioned in part 4.1. Figure 10 shows the results of the simulated rise mean velocity values versus column height. As the velocity profile shows, the bubble grows at the sparger output up to the force of buoyancy is greater than the force of surface tension, and then it releases to the column. As the bubble does not have the initial velocity (gas injection rate here is sufficiently low to assume this), the initial value of drag force is zero, and thus the bubble gains a high acceleration. At the same time, increasing the velocity leads to increasing the drag force until it equals the buoyancy force, and the bubble reaches its maximum velocity. This happens in a very short time when the bubble enters.

By increasing the bubble size from 2.6 mm to 3.5 mm, the drag force increased faster, which meant that the larger bubble reached the maximum velocity faster than the small bubbles, while the value of maximum velocity decreased by an increase in the bubble diameter.

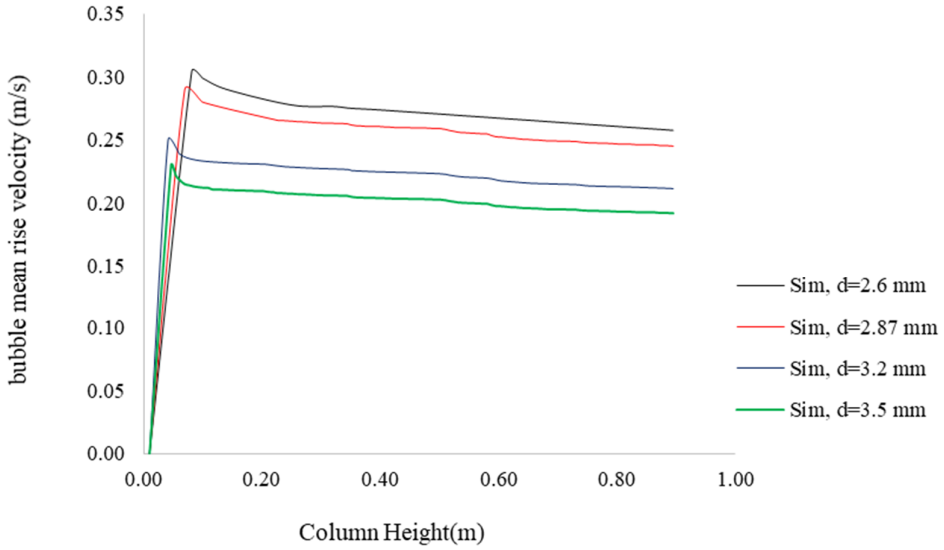

Figure 10. Bubble mean velocity profile for different bubble diameters according to the simulation results.

3.5. Discussion

The consistency of the obtained hydrodynamic parameters and component values including the bubble shape, bubble terminal velocity, and dimensionless numbers with Clift's diagram shows the accuracy of the measurements. Also the results of the simulation were validated with the experimental values, and it showed that in this work, the hydrodynamic conditions were well understood and the models were well selected in the simulation, which could be the basis for further studies.

In flotation, the bubbles play a key role. Before the bubble interactions in a bubble swarm could be understood, the behavior of single bubbles should be studied, and therefore, these studies help the researchers better recognize the bubble dynamics and their properties, which are the effective components in the performance of the flotation process. Besides, the effect of the bubble dynamics on the performance of true flotation is one of the least understood features of the flotation so it is valuable to do some additional investigation in order to develop a more comprehensive simulation model, which leads to a greater adaptation of the numerical and experimental results, which is the goal of this research team.

4. Conclusions

The single bubble motion in the flotation column was investigated in two experimental and numerical sections for the bubbly flow regime. First of all, an experiment was performed, and the bubble hydrodynamics components including the bubble rise velocity were measured using image processing. After that, the motion of a single bubble in the flotation column was simulated in two phases using the VOF model. In order to mesh verify, the simulations were performed for three mesh numbers. The results obtained were

compared for the bubble rise velocity values, and finally, with an approximation of less than 2%, mesh 2 by 752500 elements was selected and used in the simulations. Then the bubble rise velocity profile was plotted and compared with the experimental values as a validation. Furthermore, the bubble shape and terminal velocity values matched well with the Clift diagrams. In the bubble size range of the present work, with increasing bubble diameter, Reynolds increased, and the surface tension force decreased; other forces (viscosity, inertia, and compressive dynamics) increased, and the bubble shape changes from spherical to elliptical. Also the results obtained showed that the bubble motion simulation in a column flotation cell using a two-phase VOF model could predict the bubble rise velocity values with less than 5% error in comparison with the experimental results. Finally, the bubble rise velocity profile in four different diameters was presented and investigated. The results obtained showed that by increasing the bubble size from 2.6 mm to 3.8 mm, the drag force increased faster, which meant that the larger bubble reached the maximum velocity faster than the small bubbles, while the value of maximum velocity decreased by an increase in the bubble diameter.

Acknowledgments

The authors gratefully acknowledge the manager of the Ultrafast Processing and Computing Center of the University of Kashan for performing the simulations and Dr. Mohsen Karimi for his valuable guidance.

References

[1]. Wang, G., Ge, L., Mitra, S., M. Evans, G., Joshi, J. and Chen, S. (2018). A review of CFD modeling studies on the flotation process. 127 (153–177).

[2]. Deng, H., Mehta, R. and Warren, G. (1996). Numerical modeling of flows in flotation columns. Int J Miner Process, 48(1), 61-72.

[3]. Xia, Y., Peng, F. and Wolfe, E. (2006). CFD simulation of alleviation of fluid back mixing by baffles in bubble column. Minerals Eng. 19 (9): 925-37.

[4]. Chakraborty, D., Guha, M. and Banerjee, P. (2009). CFD simulation on influence of superficial gasvelocity, column size, sparger arrangement, and taper angle on hydrodynamics of the column flotation cell. Chem Eng Commun. 9 (196): 1102-16.

[5]. Nadeem, M., Ahmed, J., Chughtai, I. and Ullah, A. (2009). CFD-based estimation of collision probabilities between fine particles and bubbles having intermediate Reynolds number. Nucleus. 46 (3): 153-159.

[6]. Koh, P. and Schwarz, M. (2009). CFD models of microcel and Jameson flotation cells. Seventh international conference on CFD in the minerals and process industries, CSIRO. Melbourne, Australia.

[7]. Rehman, A., Nadeem, M., Zaman, M. and Nadeem, B. (2011). Effect of various baffle designs on air holdup and mixing in a flotation column using CFD. 8th International Bhurban Conference on Applied Sciences and Technology, Islamabad, Pakistan.

[8]. Sahbaz, O., Ercetin, U. and Oteyaka, B. (2012). Determination of turbulence and upper size limit in Jameson flotation cell by the use of computational fluid dynamic modelling Physicochem. 48 (533–544).

[9]. Yan, X., Liu, J., Cao, Y. and Wang, L. (2012). A single-phase turbulent fl ow numerical simulation of a cyclonic-static micro bubble flotation column. Int. J. Miner. Process. 22: 95-100.

[10]. Gong, M., Li, C. and Li, Z. (2015). Numerical analysis of flow in a highly efficient flotation column. Asia-Pac. J. Chem. Eng, 10, 84–95.

[11]. Wang, A., Yan, X., Wang, L., Cao, Y. and Liu, J. (2015). Effect of cone angles on single-phase flow of a laboratory cyclonic-static micro-bubble flotation column: PIV measurement and CFD simulations. Sep. Purif. Technol, 149, 308–314.

[12]. Sarhan, A., Naser, J. and Brooks, G. (2016). CFD simulation on influence of suspended solid particles on bubbles' coalescence rate in flotation cell. Int J Miner Process. 146: 54-64.

[13]. Cai, X., Chen, J., Liu, M., Ji, Y., Ding, G. and Zhang, L. (2016). CFD simulation of oil-water separation characteristics in a compact flotation unit by population balance modeling. J. Disper. Sci. Technol, 38, 1435–1447.

[14]. Cai, X., Chen, J., Liu, M., Ji, Y. and An, S. (2017). Numerical studies on dynamic characteristics of oil-water separation in loop flotation column using a population balance model. Sep. Purif. Technol, 176, 134–144.

[15]. Sarhan, A., Naser, J. and Brooks, G. (2017a). Bubbly flow with particle attachment and detachment – a multi-phase CFD study. Sep. Sci. Technol, 53, 181–197.

[16]. Sarhan, A., Naser, J. and Brooks, G. (2017b). CFD analysis of solid particles properties effect in three-phase flotation column. Sep. Purif. Technol, 185, 1–9.

[17]. Zhang, M., Li, T. and Wang, G. (2017). A CFD study of the flow characteristics in a packed flotation column: implications for flotation recovery improvement. Int. J. Miner. Process, 159, 60–68.

[18]. Wang, G., Evans, G. and Jameson, G. (2017a). Bubble-particle detachment in a turbulent vortex II—computational methods. 102(58–67).

[19]. Wang, L., Wang, Y., Yan, X., Wang, A. and Cao, Y. (2017b). A numerical study on efficient recovery of fine-grained minerals with vortex generators in pipe flow unit of acyclonic-static micro-bubble flotation column, 158 (304–313).

[20]. Farzanegan, A., Khorasanizadeh, N., Sheikhzadeh, G. and Khorasanizadeh, H. (2017). Laboratory and CFD investigations of the two-phase flow behavior in flotation columns equipped with vertical baffle. International Journal of Mineral Processing, 17, 71-83.

[21]. Yang, G., Guo, K. and Wang, T. (2017). Numerical simulation of the bubble column at elevated pressure with a CFD-PBM coupled model. Chemical Engineering Science.

[22]. Sarhan, A.R., Naser, J. and Brooks, G. (2018): CFD model simulation of bubble surface area flux in flotation column reactor in presence of minerals. International Journal of Mining Science and Technology, 28, 6, 999-1007.

[23]. Schwarz, M.P., Koh, P.T.L., Wu, J., Nguyen, B. and Zhu, Y. (2019): Modelling and measurement of multi-phase hydrodynamics in the Outotec flotation cell. Minerals Engineering, 144.

[24]. Nasirimoghaddam, S.M., Mohebbi, A., Karimi, M. and Yarahmadi, M.R. (2020). Assessment of pH-responsive nanoparticles performance on laboratory column flotation cell applying a real ore feed. International Journal of Mining Science and Technology, 30, 2, 197-205.

[25]. Yang, M., Del Pozo, D.F., Torfs, E., Rehman, U., Yu, D. and Nopens, I. (2021): Numerical simulation on the effects of bubble size and internal structure on flow behavior in a DAF tank: A comparative study of CFD and CFD-PBM approach. Chemical Engineering Journal Advances, 7.

[26]. Yan, X., Yao, Y., Meng, S., Zhao, S., Wang, L., Zhang, H. and Cao, Y. (2021): Comprehensive particle image velocimetry measurement and numerical model validations on the gas-liquid flow field in a lab-scale cyclonic flotation column. Chemical Engineering Research and Design, 174, 1-10.

[27]. Clift, R. and Grace, J. (1978). Bubbles, drops, and particles. Academic Press.

[28]. Brennen, C.E. (2005). Fundamentals of Multiphase Flows. Cambridge University Press.

[29]. Cano-Lozano, J., Bolaños-Jiménez, R., Gutiérrez-Montes, C. and Martínez-Bazán, C. (2014). The use of Volume of Fluid technique to analyze multiphase flows: specific case of bubble rising in still liquids.

[30]. URL: http://www.pmt.usp.br › martoran › notasmodelosgrad: ANSYS Fluent Theory Guide (2015).

[31]. Van der Pijl, S.P. (2005). Computation of Bubbly Flows with a Mass-Conserving Level-Set Method.

[32]. N. Vargaftik. (1975). Handbook of Physical Properties of Liquids and Gases, Springer.

[33]. Binder, R.C. (1973). Fluid mechanics. Prentice-Hall: Englewood Cliffs, N.J.

[34]. Zhang, Y., Sam, A. and Finch, J. (2003). Temperature effect on single bubble velocity profile in water and surfactant solution. Colloids and Surfaces. 223: 45-54.

[35]. Acuña, C. and Finch, J. (2010). Tracking velocity of multiple bubbles in a swarm. Vol. 94, pp. 148-157.

مطالعه تجربی و CFD بر اثر قطر اولیه حباب بر پروفیل سرعت صعود آن در سلول فلوتاسیون ستونی در مقیاس آزمایشگاهی

نرجس خراسانی‌زاده[۱]، محمد کارآموزیان[۱*] و حسین نوری بیدگلی[۲]

۱- دانشکده مهندسی معدن، نفت و ژئوفیزیک، دانشگاه صنعتی شاهرود، ایران
۲- دانشکده مهندسی مکانیک، دانشگاه آزاد اسلامی واحد کاشان، ایران

ارسال ۲۰۲۱/۰۹/۱۵، پذیرش ۲۰۲۱/۱۲/۰۶

* نویسنده مسئول مکاتبات: m.karamoozian@shahroodut.ac.ir

چکیده:

اثر قطر حباب روی پروفیل سرعت صعود آن در یک ستون فلوتاسیون با روش دینامیک سیالات محاسباتی دو فازی (CFD) مطالعه شده است. شبیه‌سازی‌ها در نرم‌افزار ANSYS® Fluent® با استفاده از مدل حجم سیال (VOF) انجام شده است. میدان محاسباتی، ستونی با مقطع مربعی با عرض ۱۰ و ارتفاع ۱۰۰ سانتی متر است و هوا به صورت تک حباب از یک اسپارجر داخلی وارد ستون می شود. هم‌چنین پارامترهای هیدرودینامیکی حین انجام آزمایش تجربی و با استفاده از روش آنالیز تصاویر ثبت شده‌اند و برای اعتبارسنجی نتایج شبیه سازی استفاده شده‌اند. نتایج نشان می‌دهد که CFD می‌تواند سرعت صعود حباب را در ستون فلوتاسیون با اختلاف کمتر از ۵ درصد در مقایسه با آزمایش تجربی پیش‌بینی کند. سپس شبیه سازی‌ها برای سایر اندازه‌های حباب در جریان حبابی، به منظور مطالعه اثر قطر حباب روی پروفیل سرعت صعود تکرار شده‌اند. نتایج به‌دست‌آمده نشان می‌دهد که حباب‌های بزرگ‌تر، سریع‌تر از حباب‌های کوچک به حداکثر سرعت خود می‌رسند، در حالی که مقدار حداکثر سرعت با افزایش قطر حباب کاهش می‌یابد. از این نتایج می‌توان برای بهبود کارایی فلوتاسیون استفاده کرد.

کلمات کلیدی: فلوتاسیون ستونی، قطر حباب، پروفیل سرعت، شبیه‌سازی چندفازی، شبیه سازی CFD.